SCIENCE CHINA
Physics, Mechanics & Astronomy

Hyperbolic metamaterial using chiral molecules

JieXing Zhao, JingJing Cheng, YingQi Chu, YanXiang Wang, FuGuo Deng and Qing Ai

Citation: SCIENCE CHINA Physics, Mechanics & Astronomy **63**, 260311 (2020); doi: 10.1007/s11433-019-1470-6

View online: http://engine.scichina.com/doi/10.1007/s11433-019-1470-6

View Table of Contents: http://engine.scichina.com/publisher/scp/journal/SCPMA/63/6

Published by the Science China Press

SCIENCE CHINA
Physics, Mechanics & Astronomy

• Article •

June 2020 Vol. 63 No. 6: 260311
https://doi.org/10.1007/s11433-019-1470-6

Hyperbolic metamaterial using chiral molecules

JieXing Zhao[1], JingJing Cheng[1], YingQi Chu[1], YanXiang Wang[1], FuGuo Deng[1,2], and Qing Ai[1*]

[1]*Department of Physics, Applied Optics Beijing Area Major Laboratory, Beijing Normal University, Beijing 100875, China;*
[2]*NAAM-Research Group, Department of Mathematics, Faculty of Science, King Abdulaziz University, Jeddah 21589, Saudi Arabia*

Received August 26, 2019; accepted October 25, 2019; published online February 21, 2020

We theoretically investigate the intra-band transitions in Möbius molecules. Due to the weak magnetic response, the relative permittivity is significantly modified by the presence of the medium while the relative permeability is not. We show that there is hyperbolic dispersion relation induced by the intra-band transitions because one of the eigen-values of permittivity possesses a different sign from the other two, while all three eigen-values of permeability are positive. We further demonstrate that the bandwidth of negative refraction is 0.165 eV for the *H*-polarized incident light, which is broader than the ones for inter-band transitions by 3 orders of magnitude. Moreover, the frequency domain has been shifted from ultra-violet to visible domain. Although there is negative refraction for the *E*-polarized incident light, the bandwidth is much narrower and depends on the incident angle.

negative refraction, hyperbolic dispersion, Möbius molecules, visible light, broad bandwidth

PACS number(s): 33.80.-b, 03.65.-w, 11.30.Rd

Citation: J. X. Zhao, J. J. Cheng, Y. Q. Chu, Y. X. Wang, F. G. Deng, and Q. Ai, Hyperbolic metamaterial using chiral molecules, Sci. China-Phys. Mech. Astron. **63**, 260311 (2020), https://doi.org/10.1007/s11433-019-1470-6

1 Introduction

Since it was theoretically proposed in 1968 [1], negative refraction has attracted broad interest because there is wide application for negative-index metamaterials [2-12], such as achieving electromagnetic-field cloaking [13, 14], facilitating sub-wavelength imaging [2], and assisting crime scene investigation [15]. Various ways have been proposed to realize negative refraction. One of them is double-negative metamaterial, in which both the permittivity ε and permeability μ are simultaneously negative at the same frequencies [1, 2, 16-18]. However, it is difficult to realize negative permeability since the magnetic response is generally weaker than the electric response orders of magnitude. Therein it is the bandwidth of negative μ that determines the bandwidth of negative refraction. Another possible way to realize negative refraction is realizing hyperbolic dispersion relation [9, 19-22]. When two of the eigen-values of permittivity tensor are opposite in sign, the material can realize negative refraction if all the eigen-values of permeability tensor are positive [23, 24]. In this case, the bandwidth of negative refraction is equal to the bandwidth of negative eigen-value of ε. Since the electric response is much stronger, the bandwidth of negative refraction of hyperbolic metamaterial is much larger than that of double-negative metamaterial.

In this paper, we investigate the possibility of realizing hyperbolic dispersion in a novel kind of chiral molecules—Möbius molecule [25, 26]. Möbius strip owns novel topo-

*Corresponding author (email: aiqing@bnu.edu.cn)

logical structures in which an insect can move from one side to the other side without crossing the border [27, 28]. Previously, Möbius molecules have been suggested for metamaterials [6, 29, 30], quantum devices [31-33], dual-mode resonators and bandpass filters [34], topological insulators [35], molecular knots and engines [36], and artificial light harvesting [37, 38]. However, because it is double-negative metamaterial, the bandwidth of negative refraction in Möbius molecules is so small, e.g., 4-80 μeV [6, 12], that it might be difficult to observe. Furthermore, since it is induced by the inter-band transitions, the negative refraction is centered at the ultraviolet frequency domain. In this paper, we consider the hyperbolic dispersion induced by the intra-band transitions. Because the magnetic response is reduced by a factor of $(N/\pi)^2$, the magnetic responses in intra-band transitions decrease by one order of magnitude for $N = 12$ and thus the eigen-values of permeability are always positive around the intra-band transitions. Furthermore, because Möbius molecules are chiral, the permittivity tensor is anisotropic and thus two of its eigen-values can possess different signs. Thus, by using intra-band transitions, we can realize hyperbolic dispersion in the visible frequency domain.

2 Permittivity and permeability in Möbius medium

In this paper, we consider a general double-ring Möbius molecule which is composed of $2N$ atoms as shown in Figure 1(a). Here W and R are the radius of the carbon atom and the Möbius ring, respectively. $2W$ denotes the width of the Möbius ring. The two sub-rings of the Möbius molecule are linked end to end.

We consider the Möbius ring as the conjugated molecule

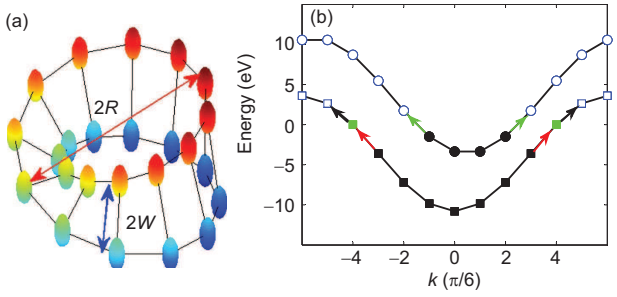

Figure 1 (Color online) (a) A double-ring Möbius molecule with $2N$ atoms and $N = 12$. (b) The energy spectrum of Möbius molecule, the black points represent the states which are filled with two electrons, the hollow points represent the states filled no electrons, and the green points represent the states filled by only one electron. The transitions denoted by arrows can take place from the initial states, which are occupied by one or two electrons, to the final states, which are not occupied by two electrons. The transitions with the same transition frequency are marked with the same color.

and thus we can use Hückel molecular orbital method to describe the coherent dynamics in the ring. Because all the atoms of Möbius ring are of the same species, the site energy difference between the two sub-rings ϵ vanishes. Thus the Hamiltonian for the single electron of the system can be written as [33]:

$$H = \sum_{j=0}^{N-1} \left[A_j^\dagger M A_j - \xi \left(A_j^\dagger A_{j+1} + \text{h.c.} \right) \right], \tag{1}$$

where

$$A_j = \begin{bmatrix} a_j \\ b_j \end{bmatrix}, \tag{2}$$

$$M = \begin{bmatrix} 0 & -V \\ -V & 0 \end{bmatrix}, \tag{3}$$

a_j (b_j) is the annihilation operator at the jth site of sub-ring a (b), V (ξ) is the inter-sub-ring (intra-sub-ring) resonant integral. Because the two sub-rings are linked end to end, the 0th atom of a (b) sub-ring is the Nth atom of b (a) sub-ring. Thus, the boundary conditions of Möbius molecular ring are given by $a_0 = b_N$ and $b_0 = a_N$. The Hamiltonian can be rewritten as:

$$H = \sum_{j=0}^{N-1} \left[B_j^\dagger V \sigma_z B_j - \xi (B_j^\dagger Q B_{j+1} + \text{h.c.}) \right], \tag{4}$$

by a local unitary transformation,

$$B_j \equiv \begin{bmatrix} c_{j\uparrow} \\ c_{j\downarrow} \end{bmatrix} = U_j A_j, \tag{5}$$

$$U_j = \frac{1}{\sqrt{2}} \begin{bmatrix} \mathrm{e}^{-\mathrm{i}\varphi_j/2} & -\mathrm{e}^{-\mathrm{i}\varphi_j/2} \\ 1 & 1 \end{bmatrix}, \tag{6}$$

where $c_{j\sigma}$ is the annihilation operator of an electron at the jth nuclear site with σ being the pseudo spin label, $\varphi_j = j\delta$, $\delta = 2\pi/N$, and

$$Q = \begin{bmatrix} \mathrm{e}^{\mathrm{i}\delta/2} & 0 \\ 0 & 1 \end{bmatrix}. \tag{7}$$

After this unitary transformation, the Möbius boundary condition can be replaced by the periodical boundary condition, i.e., $B_N = B_0$.

The Hamiltonian of Möbius ring can be diagonalized by the Fourier transform $B_j = \sum_{j=0}^{N-1} \mathrm{e}^{-\mathrm{i}kj} C_k$, with $C_k = \left[C_{k\uparrow}, C_{k\downarrow} \right]^{\mathrm{T}}$. We can obtain the two energy sub-bands, i.e.,

$$E_{k\uparrow} = V - 2\xi \cos(k - \delta/2), \tag{8}$$

$$E_{k\downarrow} = -V - 2\xi \cos k, \tag{9}$$

with eigen-states

$$|k,\uparrow\rangle = \frac{1}{\sqrt{2N}}\sum_{j=0}^{N-1} \mathrm{e}^{-\mathrm{i}(k-\delta/2)j}(a_j^\dagger - b_j^\dagger)\,|0\rangle\,, \tag{10}$$

$$|k,\downarrow\rangle = \frac{1}{\sqrt{2N}}\sum_{j=0}^{N-1} \mathrm{e}^{-\mathrm{i}kj}(a_j^\dagger + b_j^\dagger)\,|0\rangle\,, \tag{11}$$

respectively, where $|0\rangle$ is the state of vacuum, $k = 0, \pm\delta, \pm 2\delta \ldots$, $\uparrow$ and $\downarrow$ denotes the upper and lower band respectively. The energy spectrum of Möbius molecular ring is shown in Figure 1(b). Note that the upper band is symmetric with respect to $k = \delta/2$, while the lower band is symmetric with respect to $k = 0$. Due to this symmetry, the three pairs of intra-band transitions denoted by the arrows with the same color possess the same transition frequencies, respectively.

2.1 Without local field correction

In order to judge whether the material is a negative-refraction medium, we must calculate the relative permittivity $\overleftrightarrow{\varepsilon_r}$ and permeability $\overleftrightarrow{\mu_r}$ for the same incident frequency. According to ref. [39], the electric displacement field $\mathbf{D}$ could be given as:

$$\mathbf{D} = \varepsilon_0 \overleftrightarrow{\varepsilon_r}\mathbf{E} = \varepsilon_0\mathbf{E} + \mathbf{P}, \tag{12}$$

where ε_0 is the permittivity of vacuum, $\mathbf{E}$ is the applied electric field, $\mathbf{P}$ is the polarization field. And the magnetic induction $\mathbf{B}$ is

$$\mathbf{B} = \mu_0\,(\mathbf{H} + \mathbf{M}) = \mu_0 \overleftrightarrow{\mu_r}\mathbf{H}, \tag{13}$$

where μ_0 is the permeability of vacuum, $\mathbf{H}$ is the applied magnetic field, $\mathbf{M}$ is the magnetization field. Under the dipole approximation [39], according to the linear response theory [40], we can obtain

$$\mathbf{P} = -\sum_{i\neq f}\frac{n_i\mathbf{d}_{if}\mathbf{d}_{fi}\cdot\mathbf{E}\,(t)}{\left(n_f+1\right)\hbar v_0}\mathrm{Re}\left(\frac{1}{\omega-\triangle_{fi}+\mathrm{i}\gamma}\right), \tag{14}$$

$$\mathbf{M} = -\sum_{i\neq f}\frac{n_i\mu_0\mathbf{m}_{if}\mathbf{m}_{fi}\cdot\mathbf{H}\,(t)}{\left(n_f+1\right)\hbar v_0}\mathrm{Re}\left(\frac{1}{\omega-\triangle_{fi}+\mathrm{i}\gamma}\right), \tag{15}$$

where n_i and n_f are the number of electrons occupying in the initial and final states respectively, $\triangle_{fi}$ is the transition frequency between the final state $|f\rangle$ and the initial state $|i\rangle$, $\mathbf{d}_{if} = \langle i|\,\mathbf{d}\,|f\rangle$ and $\mathbf{m}_{if} = \langle i|\,\mathbf{m}\,|f\rangle$ are the matrix elements of electric dipole $\mathbf{d}$ and magnetic dipole $\mathbf{m}$ between the initial and final states, $v_0 \simeq 2\pi(R+W)^2W$ is the volume occupied by a Möbius molecule, ω is the frequency of incident light, γ^{-1} is the lifetime of the excited states. Inserting eqs. (14) and (15) into eqs. (12) and (13), respectively, the relative permittivity and permeability could be obtained as:

$$\overleftrightarrow{\varepsilon_r} = 1 - \sum_{i\neq f}\frac{n_i\mathbf{d}_{if}\mathbf{d}_{fi}}{\left(n_f+1\right)\hbar\varepsilon_0 v_0}\mathrm{Re}\left(\frac{1}{\omega-\triangle_{fi}+\mathrm{i}\gamma}\right), \tag{16}$$

$$\overleftrightarrow{\mu_r} = 1 - \sum_{i\neq f}\frac{n_i\mu_0\mathbf{m}_{if}\mathbf{m}_{fi}}{\left(n_f+1\right)\hbar v_0}\mathrm{Re}\left(\frac{1}{\omega-\triangle_{fi}+\mathrm{i}\gamma}\right). \tag{17}$$

Because the size of the molecule is much smaller than the wavelength of the incident light, it is valid to write the interaction Hamiltonian between the molecule and the incident light under dipole approximation [39], i.e.,

$$H_E = -\mathbf{d}\cdot\mathbf{E}\cos\omega t. \tag{18}$$

We assume that

$$\left\langle\phi_{js}\right|\mathbf{r}\left|\phi_{j's'}\right\rangle = \delta_{jj'}\delta_{ss'}\mathbf{R}_{js}, \tag{19}$$

where $\left|\phi_{j+}\right\rangle = a_j^\dagger|0\rangle$, $\left|\phi_{j-}\right\rangle = b_j^\dagger|0\rangle$, $\mathbf{R}_{j+}\left(\mathbf{R}_{j-}\right)$ is the position of the jth nuclear in a (b) sub-ring which can be given by

$$\begin{aligned}\mathbf{R}_{j\pm} =& \left(R \pm W\sin\frac{\varphi_j}{2}\right)\cos\varphi_j\hat{e}_x \\ &+ \left(R \pm W\sin\frac{\varphi_j}{2}\right)\sin\varphi_j\hat{e}_y \pm W\cos\frac{\varphi_j}{2}\hat{e}_z,\end{aligned} \tag{20}$$

where $\varphi_j = j\delta$ is the azimuthal angle of the jth nucleus. By using eqs. (18)-(20), we can obtain the matrix elements of H_E between the eigen-states of H which are written as eqs. (10) and (11). Here, we only give the matrix elements of intra-band transitions as follows:

$$\langle k,\uparrow|H_E\,|k\pm\delta,\uparrow\rangle = \frac{eR}{2}\left(E^{(x)} \mp \mathrm{i}E^{(y)}\right)\cos\omega t, \tag{21}$$

$$\langle k,\downarrow|H_E\,|k\pm\delta,\downarrow\rangle = \frac{eR}{2}\left(E^{(x)} \mp \mathrm{i}E^{(y)}\right)\cos\omega t, \tag{22}$$

$$\langle k,\sigma|H_E\,|k\pm 2\delta,\sigma\rangle = 0, \tag{23}$$

where $\sigma = \downarrow,\uparrow$. We can summarize the intra-band transition selection rules for the electric-dipole operator from these matrix elements of H_E as:

$$|k,\sigma\rangle \overset{x,y}{\rightleftharpoons} |k\pm\delta,\sigma\rangle\,. \tag{24}$$

Similarly, we can obtain the matrix elements of the interaction Hamiltonian under dipole approximation [39]:

$$H_B = -\mathbf{m}\cdot\mathbf{B}\cos\omega t \tag{25}$$

between the eigen-states of H. We also only give the matrix elements of intra-band transitions

$$\begin{aligned}\langle k,\uparrow|\,H_B\,|k+\delta,\uparrow\rangle =& \frac{eW^2\xi}{8\hbar}\left[\cos(k-\delta)-\cos(k+\delta)\right] \\ &\times\left(\mathrm{i}B^{(x)} + B^{(y)} - B^{(z)}\right)\cos\omega t,\end{aligned} \tag{26}$$

$$\begin{aligned}\langle k,\uparrow|\,H_B\,|k-\delta,\uparrow\rangle =& \frac{eW^2\xi}{8\hbar}\left[\cos(k-2\delta)-\cos k\right] \\ &\times\left(\mathrm{i}B^{(x)} - B^{(y)} + B^{(z)}\right)\cos\omega t,\end{aligned} \tag{27}$$

$$\langle k,\uparrow|H_B|k+2\delta,\uparrow\rangle = \frac{eW^2\xi}{8\hbar}\left[\cos k-\cos(k+\delta)\right] \times\left(\mathrm{i}B^{(x)}+B^{(y)}\right)\cos\omega t, \tag{28}$$

$$\langle k,\downarrow|H_B|k+\delta,\downarrow\rangle = \frac{eW^2\xi}{8\hbar}\left[\cos\left(k-\frac{\delta}{2}\right)-\cos\left(k+\frac{3\delta}{2}\right)\right] \times\left(\mathrm{i}B^{(x)}+B^{(y)}-B^{(z)}\right)\cos\omega t, \tag{29}$$

$$\langle k,\downarrow|H_B|k-\delta,\downarrow\rangle = \frac{eW^2\xi}{8\hbar}\left[\cos\left(k-\frac{3\delta}{2}\right)-\cos\left(k+\frac{\delta}{2}\right)\right] times\left(-\mathrm{i}B^{(x)}+B^{(y)}-B^{(z)}\right)\cos\omega t, \tag{30}$$

$$\langle k,\downarrow|H_B|k+2\delta,\downarrow\rangle = \frac{eW^2\xi}{8\hbar}\left[\cos\left(k+\frac{\delta}{2}\right)-\cos\left(k+\frac{3\delta}{2}\right)\right] \times\left(\mathrm{i}B^{(x)}+B^{(y)}\right)\cos\omega t. \tag{31}$$

Furthermore, the selection rules for the magnetic-dipole operator are

$$|k,\sigma\rangle \overset{x,y,z}{\rightleftharpoons} |k\pm\delta,\sigma\rangle,\ |k,\sigma\rangle \overset{x,y}{\rightleftharpoons} |k+2\delta,\sigma\rangle. \tag{32}$$

Notice that as the matrix elements of H_B for intra-band transitions are proportional to W^2 and those for inter-band transitions are $O(RW)$, the magnetic responses for intra-band transitions have been reduced by a factor of $(R/W)^2 = (N/\pi)^2$. Hereafter, we will show by numerical simulation that the eigen-values of permeability tensor are always positive around the intra-band transitions.

According to eqs. (24) and (32), only the transitions $|k,\sigma\rangle \rightleftharpoons |k\pm\delta,\sigma\rangle$ are allowed by both electric and magnetic dipole couplings. Moreover, a transition can take place when the initial state is non-empty (NE) and the final state is not fully filled with electrons (NFF). And we only consider intra-band transitions. Considering all the conditions above, only six transitions, depicted by the arrows in Figure 1(b), are considered in this paper. We divide these transitions into three pairs by the same transition frequencies respectively: (1) $|\delta,\uparrow\rangle \rightleftharpoons |2\delta,\uparrow\rangle$, $|-\delta,\uparrow\rangle \rightleftharpoons |-2\delta,\uparrow\rangle$, denoted by the green arrows; (2) $|3\delta,\downarrow\rangle \rightleftharpoons |4\delta,\downarrow\rangle$, $|-3\delta,\downarrow\rangle \rightleftharpoons |-4\delta,\downarrow\rangle$, denoted by the red arrows; (3) $|4\delta,\downarrow\rangle \rightleftharpoons |5\delta,\downarrow\rangle$, $|-4\delta,\downarrow\rangle \rightleftharpoons |-5\delta,\downarrow\rangle$, denoted by the black arrows. We can calculate the elements of the dielectric tensor by eq. (16), with the nonvanishing matrix elements being

$$\varepsilon_r^{xx}=\varepsilon_r^{yy}=1-\sum_{(k\sigma)\in\mathrm{NE}}\sum_{(k'\sigma)\in\mathrm{NFF}}\eta_{kk'\sigma}, \tag{33}$$

$$\varepsilon_r^{yx}=-\varepsilon_r^{xy} =\eta'_{2\delta,3\delta,\uparrow}-\eta'_{-\delta,-2\delta,\uparrow}+\sum_{k=3\delta,4\delta}\left(\eta'_{k,k+\delta,\downarrow}-\eta'_{-k,-k-\delta,\downarrow}\right), \tag{34}$$

where

$$\eta_{kk'\sigma}=\frac{n_i e^2R^2}{4\left(n_f+1\right)\hbar\varepsilon_0 v_0}\frac{1}{\omega-\triangle_{kk'\sigma}+\mathrm{i}\gamma} \tag{35}$$

and $\Delta_{kk'\sigma}$ is the transition frequency between the final state $|k'\sigma\rangle$ and the initial state $|k\sigma\rangle$ within the same band σ, $\eta'_{kk'\sigma}$ is the real part of $\eta_{kk'\sigma}$.

Eq. (35) indicates that if two transitions share the same transition frequency $\Delta_{kk'\sigma}$, they would also possess the same $\eta_{kk'\sigma}$. Since there are three pairs of transitions which possess the same transition frequency, we can obtain three equations:

$$\begin{aligned}\eta_{2\delta,3\delta,\uparrow}&=\eta_{-\delta,-2\delta,\uparrow},\\ \eta_{3\delta,4\delta,\downarrow}&=\eta_{-3\delta,-4\delta,\downarrow},\\ \eta_{4\delta,5\delta,\downarrow}&=\eta_{-4\delta,-5\delta,\downarrow}.\end{aligned} \tag{36}$$

Inserting these three equations into eq. (34), we find that the off-diagonal elements $\varepsilon_r^{xy}=\varepsilon_r^{yx}=0$. As a result, $\overleftrightarrow{\varepsilon_r}$ can be simplified as:

$$\overleftrightarrow{\varepsilon_r}=\begin{bmatrix}1-\eta' & 0 & 0\\ 0 & 1-\eta' & 0\\ 0 & 0 & 1\end{bmatrix}, \tag{37}$$

where $\eta'=\sum_{(k\sigma)\in\mathrm{NE}}\sum_{(k'\sigma)\in\mathrm{NFF}}\eta'_{kk'\sigma}$. The three eigen-values of $\overleftrightarrow{\varepsilon_r}$ are $\varepsilon_r^{xx}=\varepsilon_r^{yy}=1-\eta'$ and $\varepsilon_r^{zz}=1$. Obviously, one of the eigen-values of $\overleftrightarrow{\varepsilon_r}$ is identical to 1. Figure 2 numerically demonstrates the relation between $\varepsilon_r^{xx}\left(\varepsilon_r^{yy}\right)$ and the detuning $\Delta\omega=\omega-\Delta_{kk'\sigma}$. The illustration presents the situation when the detuning is less than 100 μeV, while the inset shows the relation in the large-detuning regime. We can obtain that the bandwidth of negative permittivity is about 1.65×10^5 μeV, which is broader than the previous discovery in ref. [12] by 3 orders of magnitude.

From eq. (35), the real part of $\eta_{kk'\sigma}$ could be re-expressed

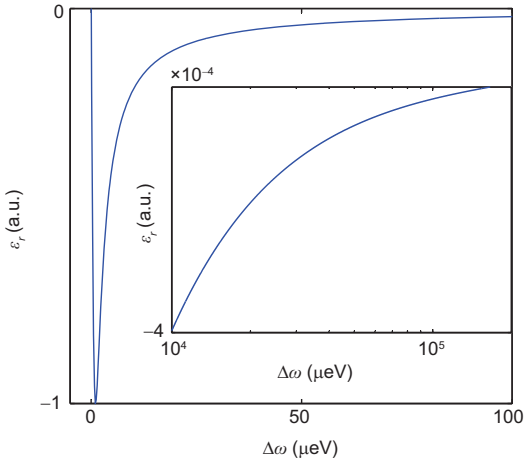

Figure 2 (Color online) The relationship between ε_r and the detuning $\Delta\omega$ around the transition frequency 2.6353829 eV without local field correction. Here we adopt the following parameters: $V=\xi$ =3.6 eV [41], W =0.077 nm [42], $R=NW/\pi$, γ^{-1} =4 ns [43].

as:

$$\eta'_{kk'\sigma} = \frac{n_i e^2 R^2}{4\left(n_f+1\right)\varepsilon_0 v_0}\left(\Delta\omega_{kk'\sigma} + \frac{\gamma^2}{\Delta\omega_{kk'\sigma}}\right)^{-1}, \tag{38}$$

where $\Delta\omega_{kk'\sigma} = \omega - \Delta_{kk'\sigma}$. On account of the initial and final conditions, it can be explicitly written as:

$$\eta' = \frac{e^2R^2}{2\varepsilon_0 v_0}\left[\left(\Delta\omega_{4\delta,5\delta,\downarrow} + \frac{\gamma^2}{\Delta\omega_{4\delta,5\delta,\downarrow}}\right)^{-1} + 2\left(\Delta\omega_{2\delta,3\delta,\uparrow} + \frac{\gamma^2}{\Delta\omega_{2\delta,3\delta,\uparrow}}\right)^{-1} + \left(\Delta\omega_{3\delta,4\delta,\downarrow} + \frac{\gamma^2}{\Delta\omega_{3\delta,4\delta,\downarrow}}\right)^{-1}\right]. \tag{39}$$

To find the bandwidth of negative ε_r, we should find the two solutions to the equation:

$$1 - \eta'(\omega) = 0. \tag{40}$$

For the solution between $\omega_{2\delta,3\delta,\uparrow} = 3.2276717$ eV and $\omega_{4\delta,5\delta,\downarrow} = 2.6353829$ eV, which yields $\Delta\omega_{3\delta,4\delta,\downarrow} \gg \Delta\omega_{2\delta,3\delta,\uparrow}, \Delta\omega_{4\delta,5\delta,\downarrow}$, eq. (39) could be simplified as:

$$\eta' \simeq \frac{e^2R^2}{2\varepsilon_0 v_0}\left[\left(\Delta\omega_{4\delta,5\delta,\downarrow} + \frac{\gamma^2}{\Delta\omega_{4\delta,5\delta,\downarrow}}\right)^{-1} + 2\left(\Delta\omega_{2\delta,3\delta,\uparrow} + \frac{\gamma^2}{\Delta\omega_{2\delta,3\delta,\uparrow}}\right)^{-1}\right]. \tag{41}$$

For the present parameters, we find $\gamma \sim 10^{-6}$ eV and $C = \frac{e^2R^2}{2\varepsilon_0 v_0} \sim 11.4$ eV. When $\Delta\omega_{2\delta,3\delta,\uparrow}$ and $\Delta\omega_{4\delta,5\delta,\downarrow} \gg \gamma$ is satisfied, the terms of γ^2 could be ignored, and thus

$$\eta' \simeq C\left(\frac{1}{\Delta\omega_{4\delta,5\delta,\downarrow}} + \frac{2}{\Delta\omega_{2\delta,3\delta,\uparrow}}\right). \tag{42}$$

Inserting the above equation into eq. (40), we obtain the solution $\omega_1 = 2.8305463$ eV while the other solution $\omega = 37.23251$ eV should be discarded because it is far away from the transition. To find the solution around the resonance frequency $\omega = 2.6353829$ eV, we simplify η' as:

$$\eta' = C\left(\Delta\omega_{4\delta,5\delta,\downarrow} + \frac{\gamma^2}{\Delta\omega_{4\delta,5\delta,\downarrow}}\right)^{-1}. \tag{43}$$

Inserting eq. (43) into eq. (40) yields $\Delta\omega_{4\delta,5\delta,\downarrow} \simeq 0$ as $C^2 \gg \gamma^2$. The other solution $\Delta\omega_{4\delta,5\delta,\downarrow} \simeq C$ should be discarded because it is not close to the transition. Thus, the other solution to eq. (40) is $\omega_2 = 2.6353829$ eV. We obtain the window of negative permittivity is $\Delta\omega = \omega_1 - \omega_2 = 0.1952$ eV, which is consistent with the numerical simulation in Figure 2.

In the same way, we can calculate the elements of the permeability tensor $\overleftrightarrow{\mu_r}$ by using eq. (17) as:

$$\overleftrightarrow{\mu_r} = \begin{pmatrix} 1-\beta & -\mathrm{i}\beta_1 & \mathrm{i}\beta_1 \\ \mathrm{i}\beta_1 & 1-\beta & \beta \\ -\mathrm{i}\beta_1 & \beta & 1-\beta \end{pmatrix}, \tag{44}$$

where $\beta = \sum_{(k\sigma)\in\mathrm{NE}}\sum_{(k'\sigma)\in\mathrm{NFF}}\alpha^2_{kk'\sigma}\eta'_{kk'\sigma}$, and

$$\beta_1 = \alpha^2_{2\delta,3\delta,\uparrow}\eta'_{2\delta,3\delta,\uparrow} - \alpha^2_{-\delta,-2\delta,\uparrow}\eta'_{-\delta,-2\delta,\uparrow} + \sum_{k=3\delta,4\delta}\left(\alpha^2_{k,k+\delta',\downarrow}\eta'_{k,k+\delta,\downarrow} - \alpha^2_{-k,-k-\delta',\sigma}\eta'_{-k,-k-\delta,\downarrow}\right), \tag{45}$$

$$\alpha_{k,k+\delta,\uparrow} = \frac{W^2\xi}{4\hbar cR}\left[\cos(k-\delta) - \cos(k+\delta)\right], \tag{46}$$

$$\alpha_{k,k-\delta,\uparrow} = \frac{W^2\xi}{4\hbar cR}\left[\cos(k-2\delta) - \cos(k)\right], \tag{47}$$

$$\alpha_{k,k+\delta,\downarrow} = \frac{W^2\xi}{4\hbar cR}\left[\cos\left(k-\frac{\delta}{2}\right) - \cos\left(k+\frac{3\delta}{2}\right)\right], \tag{48}$$

$$\alpha_{k,k-\delta,\downarrow} = \frac{W^2\xi}{4\hbar cR}\left[\cos\left(k-\frac{3\delta}{2}\right) - \cos\left(k+\frac{\delta}{2}\right)\right]. \tag{49}$$

According to eq. (47), we can obtain the following three relations:

$$\alpha^2_{2\delta,3\delta,\uparrow} = \alpha^2_{-\delta,-2\delta,\uparrow}, \tag{50}$$

$$\alpha^2_{3\delta,4\delta,\downarrow} = \alpha^2_{-3\delta,-4\delta,\downarrow}, \tag{51}$$

$$\alpha^2_{4\delta,5\delta,\downarrow} = \alpha^2_{-4\delta,-5\delta,\downarrow}. \tag{52}$$

Inserting eqs. (51) and (36) into eq. (45), we can obtain $\beta_1 = 0$. Therefore, $\overleftrightarrow{\mu_r}$ could be simplified as:

$$\overleftrightarrow{\mu_r} = \begin{pmatrix} 1-\beta & 0 & 0 \\ 0 & 1-\beta & \beta \\ 0 & \beta & 1-\beta \end{pmatrix}. \tag{53}$$

The permeability tensor is not diagonal in the molecular coordinate system as shown above. As a result, $\overleftrightarrow{\varepsilon_r}$ and $\overleftrightarrow{\mu_r}$ cannot be simultaneously diagonalized by the same rotation transformation.

The permeability possess three eigen-values, i.e., $\mu_1 = 1 - 2\beta$, $\mu_2 = 1 - \beta$ and $\mu_3 = 1$. Because $\alpha_{kk'\sigma} \sim 10^{-3}$, μ_j's ($j = 1, 2, 3$) are generally less significantly influenced by the medium than ε_r^{jj}'s ($j = x, y, z$). This prediction is numerically confirmed in Figure 3. As shown, all eigen-values of μ_r are positive.

2.2 Local field correction

In the above sections, we obtain the relative permittivity and permeability by the linear response theory. However, because all molecules in the medium are polarized by the applied fields, the total field experienced by a molecule is the sum of the external field $\mathbf{E}$ and internal field $\mathbf{E}_\mathrm{i}$ [39], i.e.,

$$\mathbf{E}_\mathrm{tot} = \mathbf{E} + \mathbf{E}_\mathrm{i}. \tag{54}$$

And internal field could be written as $\mathbf{E}_\mathrm{i} = \mathbf{E}_\mathrm{near} - \mathbf{E}_\mathrm{mean}$, where $\mathbf{E}_\mathrm{near}$ is the electric field produced by nearby molecules and $\mathbf{E}_\mathrm{mean}$ is the mean field, which is evaluated as:

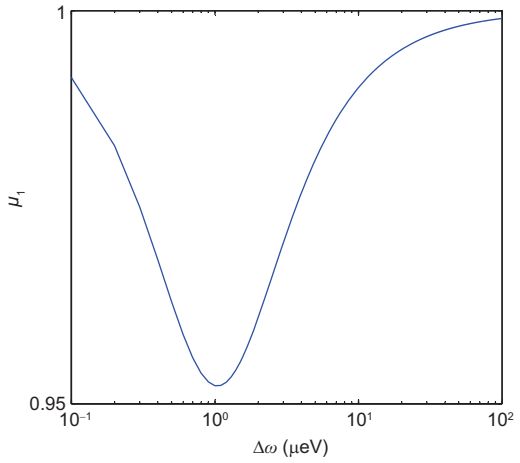

Figure 3 (Color online) The relationship between μ_1 and the detuning $\triangle\omega$ around the transition frequency 2.6353829 eV without local field correction. Here we adopt the following parameters: $V = \xi$ =3.6 eV [41], W =0.077 nm [42], $R = NW/\pi$, γ^{-1} =4 ns [43].

$$\mathbf{E}_{\text{mean}} = -\frac{1}{3\varepsilon_0}\sum_l \frac{\mathbf{p}_l}{V}, \tag{55}$$

where $\mathbf{p}_l$ is the induced dipole moment of the lth molecule inside the volume V. For a sufficiently-weak field, the induced dipole moment is given by

$$\mathbf{p}_l = \varepsilon_0\gamma_{\text{mol}}\mathbf{E}_{\text{tot}}, \tag{56}$$

where γ_{mol} is the molecular polarizability. According to linear response theory [40], the electric dipole is written as:

$$\langle\mathbf{d}\rangle = -\sum_{i\neq f}\frac{\mathbf{d}_{if}\mathbf{d}_{fi}\cdot\mathbf{E}_{\text{tot}}}{\hbar}\text{Re}\left(\frac{1}{\omega-\triangle_{fi}+\text{i}\gamma}\right). \tag{57}$$

Because $\mathbf{p}_l = \langle\mathbf{d}\rangle$, due to eqs. (57) and (56), we can obtain

$$\gamma_{\text{mol}} = -\sum_{i\neq f}\frac{\mathbf{d}_{if}\mathbf{d}_{fi}}{\hbar\varepsilon_0}\text{Re}\left(\frac{1}{\omega-\triangle_{fi}+\text{i}\gamma}\right). \tag{58}$$

The polarization $\mathbf{P} = \sum_l \mathbf{p}_l/V$ could be written as:

$$\mathbf{P} = \frac{\mathbf{p}_l}{\upsilon_0}, \tag{59}$$

if we assume identical contributions from all molecules. And the relationship between $\mathbf{P}$ and the electric field is

$$\mathbf{P} = \varepsilon_0\overleftrightarrow{\chi_e}\mathbf{E}. \tag{60}$$

By combining eqs. (56), (59) and (60), we have

$$\overleftrightarrow{\chi_e} = \left(1-\frac{\gamma_{\text{mol}}}{3\upsilon_0}\right)^{-1}\frac{\gamma_{\text{mol}}}{\upsilon_0}. \tag{61}$$

Inserting eq. (12) into eq. (60), we obtain

$$\overleftrightarrow{\varepsilon_r} = 1 + \overleftrightarrow{\chi_e}. \tag{62}$$

Inserting eq. (61) into eq. (62), $\overleftrightarrow{\varepsilon_r}$ could be expressed in terms of γ_{mol} as:

$$\overleftrightarrow{\varepsilon_r} = 1 + \left(1-\frac{\gamma_{\text{mol}}}{3\upsilon_0}\right)^{-1}\frac{\gamma_{\text{mol}}}{\upsilon_0}. \tag{63}$$

Inserting eq. (58) into the above equation, we can obtain $\overleftrightarrow{\varepsilon_r}$ tensor with the nonvanishing matrix elements

$$\varepsilon_r^{xx} = \varepsilon_r^{yy} = \frac{3-2\eta'}{3+\eta'}, \tag{64}$$

$$\varepsilon_r^{zz} = 1. \tag{65}$$

It follows from eq. (64) that the bandwidth of negative permittivity, when we consider the local field effect, is determined by the solutions to

$$\eta' = \frac{3}{2}. \tag{66}$$

Comparing eq. (66) to eq. (40), we find that the bandwidth of negative permittivity is modified by local field effect only with a factor 3/2. Base on eq. (66), we present the relation between the relative permittivity modified by local field effect and the detuning in Figure 4. Comparing Figure 2 to Figure 4, we find that local field effect only slightly changes the bandwidth of negative permittivity. In the same way, we can find that local field effect only slightly changes the permeability, and the three eigen-values of permeability tensor are all positive.

3 Negative refraction with linearly-polarized incident light

In the previous section, we have calculated the relative permittivity and permeability of the Möbius medium. The rela-

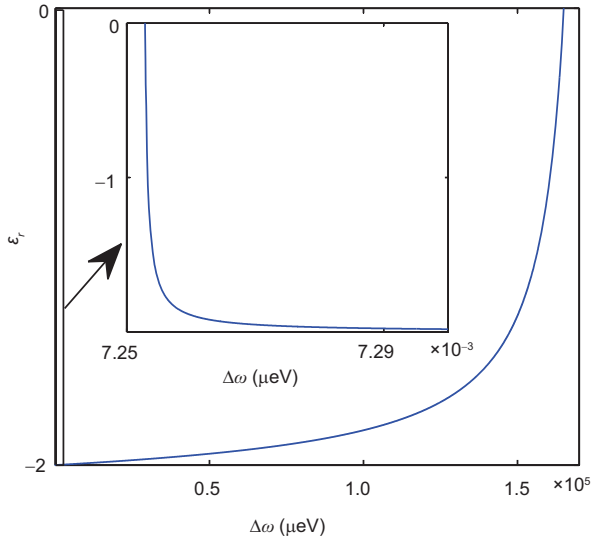

Figure 4 (Color online) ε_r^{xx} (ε_r^{yy}) modified by local field effect around the transition frequency 2.6353829 eV.

tive permittivity and permeability are second-order tensors, which are not diagonal in the same coordinate system. In this section, by both analytic and numerical simulations, we clearly show that there is hyperbolic dispersion relation in the Möbius medium, and the conditions under which the negative refraction can take place are discussed.

3.1 *H*-polarized incident configuration

As illustrated in Figure 5(a), a linearly-polarized monochromatic light is incident from the air into Möbius medium. The electric and magnetic fields of incident wave are respectively

$$\mathbf{E}_i = \left(E_{iy}\hat{e}_y + E_{iz}\hat{e}_z\right)\mathrm{e}^{\mathrm{i}(\mathbf{k}_i\cdot\mathbf{r}-\omega t)}, \tag{67}$$

$$\mathbf{H}_i = H_{ix}\hat{e}_x\mathrm{e}^{\mathrm{i}(\mathbf{k}_i\cdot\mathbf{r}-\omega t)}, \tag{68}$$

where $\mathbf{k}_i = k_{iy}\hat{e}_y + k_{iz}\hat{e}_z$ is the wave vector. We call this incident configuration as H-polarized light because the magnetic field of the incident light is perpendicular to the wave vector.

According to the boundary conditions,

$$\hat{e}_y \times (\mathbf{H}_i + \mathbf{H}_r - \mathbf{H}_t) = 0, \tag{69}$$

$$k_{tx} = k_{ix} = 0, \tag{70}$$

$$k_{tz} = k_{iz} > 0, \tag{71}$$

and eq. (68), the magnetic and electric fields of the refracted light can be written as:

$$\mathbf{H}_t = H_{tx}\hat{e}_x\mathrm{e}^{\mathrm{i}(\mathbf{k}_t\cdot\mathbf{r}-\omega t)}, \tag{72}$$

$$\mathbf{E}_t = \left(E_{ty}\hat{e}_y + E_{tz}\hat{e}_z\right)\mathrm{e}^{\mathrm{i}(\mathbf{k}_t\cdot\mathbf{r}-\omega t)}, \tag{73}$$

where the wave vector of refracted wave is $\mathbf{k}_t = k_{ty}\hat{e}_y + k_{tz}\hat{e}_z$. According to eqs. (72) and (73), the Maxwell's equations of refracted light could be written as:

$$\nabla \times \mathbf{E}_t = \mathrm{i}\omega\mu_0\overleftrightarrow{\mu_r}\mathbf{H}_t, \tag{74}$$

$$\nabla \times \mathbf{H}_t = -\mathrm{i}\omega\varepsilon_0\overleftrightarrow{\varepsilon_r}\mathbf{E}_t. \tag{75}$$

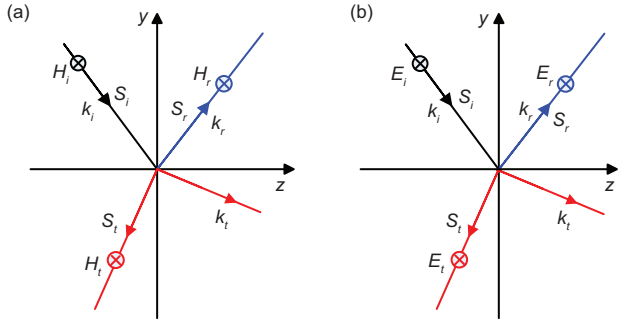

Figure 5 (Color online) Negative refraction for hyperbolic dispersion with $\varepsilon_r^{xx} < 0$, $\varepsilon_r^{yy} < 0$, and $\varepsilon_r^{zz} > 0$. (a) H-polarized incident field; (b) E-polarized incident field. The Poynting vector, wave vector and magnetic field of the incident wave are $\mathbf{S}_i$, $\mathbf{k}_i$ and $\mathbf{H}_i$, respectively. It is reflected with Poynting vector $\mathbf{S}_r$, wave vector $\mathbf{k}_r$ and magnetic field $\mathbf{H}_r$. It is transmitted with Poynting vector $\mathbf{S}_t$, wave vector $\mathbf{k}_t$ and magnetic field $\mathbf{H}_t$.

Inserting eq. (75) into eq. (74), we can obtain

$$\nabla \times \left[\left(\overleftrightarrow{\varepsilon_r}\right)^{-1}\nabla \times \mathbf{H}_t\right] = \frac{\omega^2}{c^2}\overleftrightarrow{\mu_r}\mathbf{H}_t. \tag{76}$$

For nontrivial solutions to the equation, the determinant of its coefficient matrix should be equal to zero, which yields a hyperbolic dispersion relation

$$\varepsilon_r^{yy}k_{ty}^2 + \varepsilon_r^{zz}k_{tz}^2 = \frac{\omega^2}{c^2}\varepsilon_r^{yy}\varepsilon_r^{zz}\mu_r^{xx}, \tag{77}$$

where the solutions are

$$k_{ty} = \pm\sqrt{\omega^2\varepsilon_r^{zz}\mu_r^{xx}/c^2 - \varepsilon_r^{zz}k_{tz}^2/\varepsilon_r^{yy}}. \tag{78}$$

Because $\varepsilon_r^{zz} = 1$ and $\varepsilon_r^{yy} < 0$, the real solution to eq. (78) always exists. Below, we will show that we should choose the negative solution for a correct Poynting vector of the refracted light. According to eq. (75), we can obtain

$$\mathbf{E}_t = -\frac{1}{\omega\varepsilon_0}\left(\overleftrightarrow{\varepsilon_r}\right)^{-1}(\mathbf{k}_t \times \mathbf{H}_t). \tag{79}$$

Inserting the above equation into $\mathbf{S}_t = \frac{1}{2}(\mathbf{E}_t \times \mathbf{H}_t^*)$, the Poynting vector of refracted light could be written as $\mathbf{S}_t = S_{ty}\hat{e}_y + S_{tz}\hat{e}_z$ with

$$S_{ty} = \frac{k_{ty}H_{tx}^2}{2\omega\varepsilon_0\varepsilon_r^{zz}}, \tag{80}$$

$$S_{tz} = \frac{k_{tz}H_{tx}^2}{2\omega\varepsilon_0\varepsilon_r^{yy}}. \tag{81}$$

As shown in Figure 5(a), the condition under which the refracted light can propagate in the medium is $S_{ty} < 0$. Because $\varepsilon_r^{zz} = 1 > 0$, according to eq. (80), we should take the negative solution in eq. (78) to meet the criterion $S_{ty} < 0$. According to the boundary conditions in eq. (70), we can obtain from eq. (81) that $S_{tz} < 0$ as $\varepsilon_r^{yy} < 0$. Because the Poynting vectors of incident and refracted lights are on the same side of the normal, negative refraction is realized. The bandwidth of negative refraction is given by the bandwidth of negative ε_r^{yy}, i.e., 0.165 eV.

3.2 *E*-polarized incident configuration

Analogously, we consider an E-polarized incident configuration, i.e.,

$$\mathbf{E}_i = E_{ix}\hat{e}_x\mathrm{e}^{\mathrm{i}(\mathbf{k}_i\cdot\mathbf{r}-\omega t)}, \tag{82}$$

$$\mathbf{H}_i = \left(H_{iy}\hat{e}_y + H_{iz}\hat{e}_z\right)\mathrm{e}^{\mathrm{i}(\mathbf{k}_i\cdot\mathbf{r}-\omega t)}, \tag{83}$$

where $\mathbf{k}_i = k_{iy}\hat{e}_y + k_{iz}\hat{e}_z$, $\mathbf{E}_i$ and $\mathbf{H}_i$ are the electric and magnetic fields of incident wave, respectively. In a similar way of obtaining eq. (76), we can obtain the equation

$$\nabla \times \left[\left(\overleftrightarrow{\mu_r}\right)^{-1}\nabla \times \mathbf{E}_t\right] = \frac{\omega^2}{c^2}\overleftrightarrow{\varepsilon_r}\mathbf{E}_t. \tag{84}$$

The requirement for nontrivial solution yields the hyperbolic dispersion relation as:

$$\varepsilon_r^{yy}k_{ty}^2+\varepsilon_r^{zz}k_{tz}^2=\frac{\omega^2}{c^2}\varepsilon_r^{yy}\varepsilon_r^{zz}\mu_r^{xx}, \tag{85}$$

which is the same as eq. (77) with the same solution given by eq. (78). We can obtain the Poynting vector of refracted light $\mathbf{S}_t=S_{ty}\hat{e}_y+S_{tz}\hat{e}_z$, with

$$S_{ty}=\frac{E_{tx}^2}{2\omega\mu_0\mu_1}\left(\mu_r^{yz}k_{tz}+\mu_r^{xx}k_{ty}\right), \tag{86}$$

$$S_{tz}=\frac{E_{tx}^2}{2\omega\mu_0\mu_1}\left(\mu_r^{xx}k_{tz}+\mu_r^{yz}k_{ty}\right). \tag{87}$$

Figure 3 illustrates that $\mu_1>0$. As shown in Figure 5(b), S_{ty} must be negative, otherwise there would be no refracted light. By numerical calculation, we find that we should choose the negative sign of k_{ty} in eq. (78) to ensure $S_{ty}<0$. Figure 5(b) shows that the conditions of negative refraction are $S_{ty}<0$ and $S_{tz}<0$. Because the coefficient $E_{tx}^2/(2\omega\mu_0\mu_1)>0$, the conditions could be written as $\mu_r^{yz}k_{tz}+\mu_r^{xx}k_{ty}<0$ and $\mu_r^{xx}k_{tz}+\mu_r^{yz}k_{ty}<0$. Inserting the boundary conditions

$$k_{tx}=k_{ix}=0,\quad k_{tz}=k_{iz}=k_i\sin\theta, \tag{88}$$

where θ is the angle of incidence, and eq. (53) into eqs. (86) and (87), we plot Figure 6(a), which shows $S_{ty}<0$ and S_{tz} can change sign along with θ and $\Delta\omega$. We further plot S_{tz} vs θ and $\Delta\omega$ in Figure 6(b). As shown, when the incident angle θ is enlarged, the bandwidth of negative refraction is narrowed. Generally, the bandwidth for H-polarized incident configuration is much wider than that for E-polarized incident configuration.

4 Conclusion

In this work, we propose a new approach to realize negative refraction in chiral molecules by using hyperbolic dispersion. When we consider intra-band transitions, all of the three eigen-values of $\overleftrightarrow{\mu_r}$ are positive for the whole frequency domain, and one of the three eigen-values of $\overleftrightarrow{\varepsilon_r}$ possesses a different sign from the other two in some frequency domains. The window of negative refraction is determined by the window of negative $\overleftrightarrow{\varepsilon_r}$. Since the electric response is generally larger than the magnetic response orders of magnitude, the hyperbolic metamaterial can significantly broaden the window of negative refraction. In Möbius medium, since the transition frequencies of intra-band transition are smaller than those of the inter-band transitions, we can observe a bandwidth with 0.165 eV around ω =2.6354 eV (471.4 nm), which is in the range of visible light. Compared to the previous proposals in refs. [6, 12], the bandwidth of negative refraction has been significantly broadened by 3 orders of magnitude and the center frequency has been shifted from the ultraviolet to the visible frequency domain. Compared to that of the traditional split-ring resonator, 10 THz [44], the bandwidth of the negative refraction also has been slightly broadened.

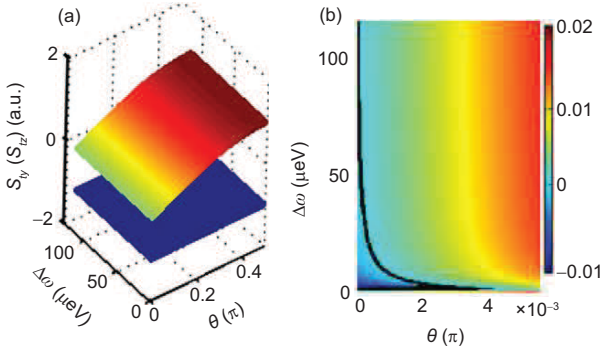

Figure 6 (Color online) (a) The dependence of S_{ty} (the lower surface) and S_{tz} (the upper surface) on $\Delta\omega$ and θ. (b) The bandwidth of negative S_{tz} vs. θ. The black line is the contour line for $S_{tz}=0$, which separates the regime $S_{tz}<0$ at the bottom-left and the regime $S_{tz}>0$ at the top-right.

This work was supported by the National Natural Science Foundation of China (Grant Nos. 11505007, 11674033, and 11474026).

1 V. G. Veselago, Sov. Phys. Usp. **10**, 509 (1968).
2 J. B. Pendry, Phys. Rev. Lett. **85**, 3966 (2000).
3 D. R. Smith, W. J. Padilla, D. C. Vier, S. C. Nemat-Nasser, and S. Schultz, Phys. Rev. Lett. **84**, 4184 (2000).
4 K. Y. Bliokh, Y. P. Bliokh, V. Freilikher, S. Savel'ev, and F. Nori, Rev. Mod. Phys. **80**, 1201 (2008).
5 A. E. Minovich, A. E. Miroshnichenko, A. Y. Bykov, T. V. Murzina, D. N. Neshev, and Y. S. Kivshar, Laser Photon. Rev. **9**, 195 (2015).
6 Y. N. Fang, Y. Shen, Q. Ai, and C. P. Sun, Phys. Rev. A **94**, 043805 (2016).
7 R. Zhao, Y. Luo, and J. B. Pendry, Sci. Bull. **61**, 59 (2016).
8 M. Khorasaninejad, and F. Capasso, Science **358**, eaam8100 (2017).
9 Q. Ai, P.-B. Li, W. Qin, C. P Sun, and F. Nori, arXiv: 1802.01280.
10 D. Felbacq, and E. Rousseau, Ann. Phys. **529**, 1600371 (2017).
11 H. Jia, W. Gao, Y. Xiang, H. Liu, and S. Zhang, Ann. Phys. **530**, 1800118 (2018).
12 J. J. Cheng, Y. Q. Chu, T. Liu, J. X. Zhao, F. G. Deng, Q. Ai, and F. Nori, J. Phys. Commun. **3**, 015010 (2019).
13 U. Leonhardt, Science **312**, 1777 (2006).
14 J. B. Pendry, D. Schurig, and D. R. Smith, Science **312**, 1780 (2006).
15 Y. Shen, and Q. Ai, Sci. Rep. **6**, 20336 (2016).
16 S. C. Zhao, Sci. China-Phys. Mech. Astron. **55**, 213 (2012).
17 Y. Shen, H. Y. Ko, Q. Ai, S. M. Peng, and B. Y. Jin, J. Phys. Chem. C **118**, 3766 (2014).
18 Y. Shen, and Y. Z. Chen, Sci. China-Phys. Mech. Astron. **60**, 070312 (2017).
19 R. K. Fisher, and R. W. Gould, Phys. Rev. Lett. **22**, 1093 (1969).
20 D. R. Smith, and D. Schurig, Phys. Rev. Lett. **90**, 077405 (2003).
21 A. Poddubny, I. Iorsh, P. Belov, and Y. Kivshar, Nat. Photon. **7**, 948 (2013).
22 S. Jahani, and Z. Jacob, Nat. Nanotech. **11**, 23 (2016).
23 S. Guan, S. Y. Huang, Y. Yao, and S. A. Yang, Phys. Rev. B **95**, 165436 (2017).
24 K. V. Sreekanth, A. De Luca, and G. Strangi, Appl. Phys. Lett. **103**, 023107 (2013).

25 E. Heilbronner, Tetrahedron Lett. **5**, 1923 (1964).
26 D. M. Walba, T. C. Homan, R. M. Richards, and R. C. Haltiwanger, New J. Chem. **17**, 661 (1993).
27 T. Yoneda, Y. M. Sung, J. M. Lim, D. Kim, and A. Osuka, Angew. Chem. Int. Ed. **53**, 13169 (2014).
28 D. Ajami, O. Oeckler, A. Simon, and R. Herges, Nature **426**, 819 (2003).
29 C. W. Chang, M. Liu, S. Nam, S. Zhang, Y. Liu, G. Bartal, and X. Zhang, Phys. Rev. Lett. **105**, 235501 (2010).
30 A. K. Poddar, and U. L. Rohde, Microwave J. **57**, 76 (2014).
31 V. Balzani, A. Credi, and M. Venturi, *Molecular Devices and Machines. Concepts and Perspectives for the Nanoworld* (VCH-Wiley, Weinheim, 2008).
32 A. Yamashiro, Y. Shimoi, K. Harigaya, and K. Wakabayashi, Physica E **22**, 688 (2004).
33 N. Zhao, H. Dong, S. Yang, and C. P. Sun, Phys. Rev. B **79**, 125440 (2009).
34 J. M. Pond, IEEE Trans. Microw. Theor. Tech. **48**, 2465 (2000).
35 Z. L. Guo, Z. R. Gong, H. Dong, and C. P. Sun, Phys. Rev. B **80**, 195310 (2009).
36 O. Lukin, and F. Vögtle, Angew. Chem. Int. Ed. **44**, 1456 (2005).
37 L. Xu, Z. R. Gong, M. J. Tao, and Q. Ai, Phys. Rev. E **97**, 042124 (2018).
38 N. Lambert, Y. N. Chen, Y. C. Cheng, C. M. Li, G. Y. Chen, and F. Nori, Nat. Phys. **9**, 10 (2013).
39 J. D. Jackson, *Classical Electrodynamics*, 2nd ed. (John Wiley, New York, 1975), p. 125.
40 R. Kubo, M. Toda, and N. Hashitsume, *Statistical Physics II Nonequilibirum Statistical Mechanics* (Springer-Verlag, Berlin, Heidelberg, 1985), pp. 109-117.
41 H. H. Greenwood, *Computing Methods in Quantum Organic Chemistry* (Wiley-InterScience, New York, 1972), p. 106.
42 R. J. Silbey, R. A. Alberty, and M. G. Bawendi, *Physical Chemistry*, 4th ed. (John Wiley&Sons, Hoboken, 2004), p. 819.
43 S. Tokuji, J. Y. Shin, K. S. Kim, J. M. Lim, K. Youfu, S. Saito, D. Kim, and A. Osuka, J. Am. Chem. Soc. **131**, 7240 (2009).
44 J. Zhou, T. Koschny, M. Kafesaki, E. N. Economou, J. B. Pendry, and C. M. Soukoulis, Phys. Rev. Lett. **95**, 223902 (2005).